Theoretical Study of Glass Systems using Molecular Electronic Structure Theory. 2. Structure and Spectroscopy of the B_2O_3 Glass

D. G. Liakos and E. D. Simandiras*

Theoretical and Physical Chemistry Institute, National Hellenic Research Foundation, 48 Vassileos Constantinou Avenue, 116 35 Athens, Greece

Received: November 30, 2007; Revised Manuscript Received: June 19, 2008

The structure and spectroscopic properties of B_2O_3 glass are examined from a theoretical point of view by using a model of 20 B_2O_3 molecules at the DFT/6-31G* level of theory and no predetermined constraints. Useful results are deduced regarding the structure, the fraction of boroxol rings, and the infrared and Raman spectra.

Introduction

Boron oxide B_2O_3 is one of the most common glass-forming materials. The molecular building block of vitreous B_2O_3 is a planar triangular BO_3 group, which arranges to form a covalent glass network. A great number of experimental and theoretical approaches give evidence for a wide variety of possibilities for the short-range order, ranging from the totally random corner-linked BO_3 triangles on one end to the planar B_3O_6 (boroxol)-ring-dominated structure at the other end.

Theoretical work on vitreous boron oxide has been focused mainly on molecular dynamics and statistical procedures,[1−6] and also a few studies based on molecular structure theory have been reported.[7−9] The main shortcoming of the latter is that either they rely on too small a size of model, due to computational limitations, or they impose initial constraints, as for example a full boroxol ring structure.

In the first part of our theoretical work on glasses,[10] we used molecular electronic structure theory calculations to find minimum energy structures and vibrational spectra for models of considerable size that correspond to and simulate the lithium metaphosphate glass. The results were very encouraging, reproducing short-range order and vibrational spectra to a very good degree of accuracy.

In this second part, we used the same methodology improved by a much better accuracy of calculation and a larger model to study the structure of the pure vitreous B_2O_3. A range of experimentally measurable quantities, that is, average coordination numbers, radial density functions, and infrared and Raman spectra, is predicted from a large model and compared to experimental data from the literature. It will be seen that from energy optimization of a large number of configurations of the cluster models, without any initial constraints, structures that reproduce very well the experimental data and the structural properties derived from experiment for vitreous B_2O_3 are obtained. This allows us to derive some useful conclusions on the structure of this glass.

Computational Details

The model chosen corresponds to the formula $(B_2O_3)_{20}$, that is, a total of 40 boron and 60 oxygen atoms are involved in the calculation. No initial constraints whatsoever were applied as they were to the short-range structure.

The computational approach has been discussed in detail elsewhere.[10] We used a small computer program to generate initial structures that were subject only to some very simple chemical constraints (such as that no two atoms can be closer than 1.30 Å). A rapid energy optimization method was then used, such as a semiempirical (PM/3) or an SCF with an STO-3G basis set. From the minima obtained in this way, we started a full energy optimization using DFT with the HCTH functional[11] and a 6-31G* basis set using the GAUSSIAN 03[12] suite of programs. The HCTH functional (in its HCTH/407 form) was chosen because the B−O molecule is included in the training set; it also proved to slightly better convergent for these models compared to the more popular B3LYP functional, giving, at the same time, very similar results. The geometry optimization at this stage is an extremely time-consuming process as the whole calculation uses, in total, 1500 contracted basis functions (2800 primitive) and, after a significant number of steps, will converge to a stationary point of the potential energy surface as this is described at the DFT/HCTH/6-31G* level. The full second derivative of the energy calculation is run at each one of these stationary points to confirm that they correspond to minima of the energy surface and to obtain the predicted vibrational infrared and Raman spectra.

All optimization calculations were run at the supercomputer center at the University of Edinburgh under a HPC-Europa grant. All force constant calculations were performed at the NHRF.

Results and Discussion

1. Structure and Bonding. ***a. Lowest Energy Structures.*** Following the procedure outlined above, over 100 initial random structures were generated. Fast semiempirical and STO-3G optimizations yielded about 50 minimum energy structures at the relevant level of theory. These were used as starting points for high-quality DFT/HCTH/6-31G* optimizations; some procedures did not converge, and from the ones that converged, the three structures that correspond to the lowest energy were chosen. These three "best" structures are labeled I, II, and III in increasing energy and are shown in Figure 1a−c, and their computed energy is given in Table 1. It is clear that for complicated structures of this size, only a view that shows the general form of the short-range order can be given; the full geometrical data as Cartesian coordinates are available from the authors and also as Supporting Information. It should be pointed out at this stage that, clearly, there is no guarantee that

* To whom correspondence should be addressed. E-mail: msim@eie.gr.

10.1021/jp711332k CCC: $40.75
Published on Web 08/05/2008

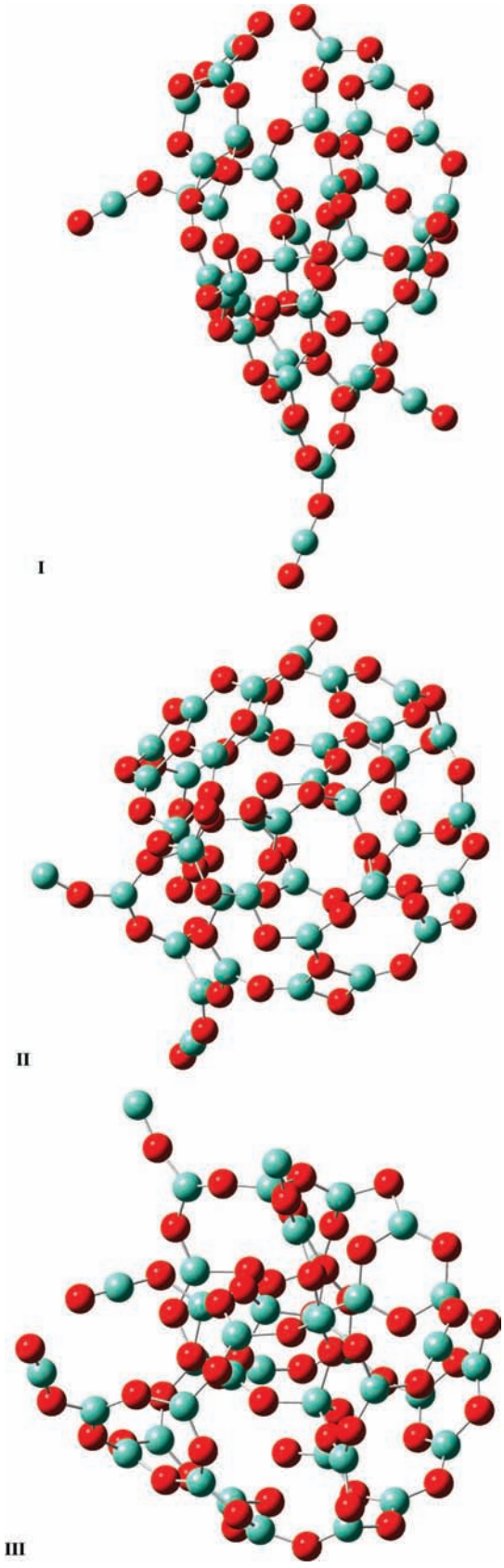

Figure 1. The shapes of the three minimum-energy structures I, II, and III (green is boron, and red is oxygen).

structures I, II, and III are the globally lowest energy stationary points of the $B_{40}O_{60}$ potential energy surface; they are simply the most stable from a significant number of structures that were tested, and as such, they should be viewed only as representative

TABLE 1: Energies in Hartree for the Three Structures and Energy Differences in kcal/mol Compared to the Lowest-Energy Structure I

structure	energy	ΔE	ΔE_0
I	−5510.870692	0	
II	−5510.684222	117.01	117.11
III	−5510.496867	234.58	229.48

structures. It will be seen in the following sections by analysis of the structural and vibrational data that there is an overall agreement with many kinds of experimental data, and hence, it is reasonable to expect that even if further computations would reach more structures with energies lying in between I and III or even lower than I, the information predicted for the structure of vitreous B_2O_3 would not change. It is interesting to note that although all glass structures are higher in energy compared to the corresponding crystalline material, the existence of a crystal-like structure is not necessary for a small cluster model. In the first part of our work,[10] the lowest energy was found for the model resembling a crystal structure, whereas in this work, no structure resembling a crystal was found; the existence of a low-energy crystal-like structure cannot be excluded but is not relevant to this investigation.

At this point, a comment on the large energy differences between the three structures is appropriate; the energy differences of Table 1 may seem large, but when the size of the cluster model is taken into account, the energy difference per B_2O_3 molecule is found to be on the order of 5 kcal/mol. This is relatively small but, of course, does not rule out the possibility that many more low-lying structures exist in between; this is discussed above and does not affect the conclusions of our work.

b. Average Coordination Number. As a first test of the computed models, we use the average coordination number of Philips and Thorpe.[13,14] Boolchand and Thorpe[15] suggest that the optimal average coordination number for covalent networks is 2.40, and that this should be true for the best glass-forming materials. Since B_2O_3 is an excellent glass former, we should expect average coordination numbers as close to 2.40 as possible.

From the optimized structures I−III, we calculate the average coordination number by assuming that a boron atom is bound to an oxygen atom if their distance is between 1.35 and 1.55 Å, which is the sum of the van der Waals distances with an uncertainty of 0.10 Å in each direction. This yields the following computed average coordination numbers: structure I: 2.22, II: 2.20, III: 2.14.

These results are close to the optimal 2.40, showing that our computed structures of the model agree very well with the proposed model for a covalent network. They also support the fact that the models are of a size that is large enough so that boundary effects (i.e., atoms near the surface of the model) do not affect significantly the overall picture. It is interesting to note that some boron atoms near the surface of the model have coordination numbers of 2, hence lower than the averages given above, which would have been even closer to the optimal 2.40 for a larger model. If we exclude the very extreme cases where boron atoms have one bond (as defined by the van der Waals radii above) or less, the computed average coordination numbers become structure I: 2.33, II: 2.24, III: 2.19.

c. Radial Distribution Function (RDF). The radial distribution function (RDF) of a glass can be obtained by various (X-ray, electron, neutron) scattering techniques and is a valuable tool for the investigation of the short-range structure of a glass. For B_2O_3 glass, the work of Bursukova et al.[16] presents a recent study, in agreement with other previous experimental works.

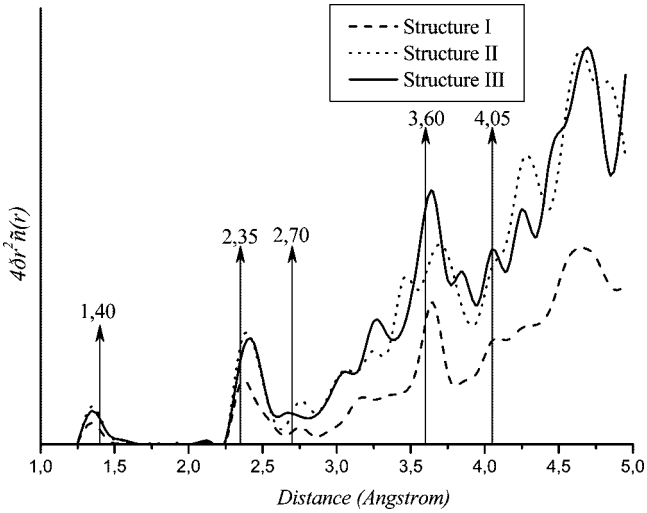

Figure 2. Radial distribution function for the three structures, with positions of experimental data given by arrows.

We use a computer program described elsewhere[17] to process the Cartesian coordinates produced by the ab initio structure optimization package and to produce a result that is directly comparable to the experimentally observed RDF. In brief, the method used is the following: for each atom in the set, the interatomic distances between it and all atoms contained in a 10 Å diameter sphere around it are tabulated. Then, the number of atoms between r and $r + dr$ for $dr = 0.1$ Å were summed and plotted against r, giving, in this way, the radial density $\rho(r)$. The radial distribution function is obtained by $D(r) = 4\pi r^3\rho(r)$.

The calculated RDFs for structures I, II, and III are given in Figure 2, and the peaks are tabulated in Table 2. It is first of all interesting to note that the general form and position of the peaks is approximately the same in the three theoretically predicted structures; it is this in conjunction with the average coordination number and the fraction of boroxol rings that will be seen later that shows that all three structures, despite their energy differences, could describe very effectively different areas of the short- and medium-range structure of the glass.

The most remarkable feature that can be seen from the comparison of our data with the experimental work of Bursukova et al.[16] in Table 2 is the very good agreement of the theoretically predicted data with the experimental interpretation of electron diffraction data. This clearly supports both the experimental interpretation and, of course, our data, which, again, the reader should be reminded, make no assumptions in the determination of the predicted structures.

d. Fraction of Boroxol Rings f. The fraction f of B atoms that belong to planar or almost planar six-membered boroxol rings in vitreous boron oxide is a highly controversial matter and one of the most heavily discussed subjects in the literature, both experimental and theoretical, on this glass. A review is presented in ref 4, where it is also claimed from an indirect molecular dynamics simulation that a theoretical value at around 0.75 is reasonable. Earlier reverse Monte Carlo simulations[3] (and see also the comment in ref 5) using neutron and X-ray diffraction data conclude that it should be less than 0.2. In their last comment,[5] Swenson and Borjenson claim that the value of 0.75 is a mere extrapolation result.

Our calculated values of f are the following for the three optimized structures: structure I: 0.375, II: 0.225, III: 0.225. At this point, it is appropriate to stress once again that no initial constraints as to the presence of boroxol rings were applied to the models, and hence, their presence (and that of larger rings) is purely a result of the energy optimization.

The values given above are the highest that have been directly calculated to date but are considerably smaller than many experimental results. It is interesting to note that the most stable structure corresponds to a higher value of f compared to the other two, but they are in no way near the values of 0.7−0.9 that have been suggested from experiment. A part of the discrepancy is due to the limited size (albeit quite large) of the model; it is not as easy to form rings near the surface of the cluster as it is in the bulk. However, a close examination of the shapes in Figure 1 reveals that there is a very clear tendency for nearly all B atoms to be part of some complete or incomplete ring; for example, in structure I, we can locate four isolated six-membered classical boroxol rings, two merged six-membered rings but also two nearly flat isolated and one bridging eight-membered rings and various other incomplete parts. Close examination of the other two structures gives a similar picture, that is, at least two eight-membered rings in each, in addition to the six-membered rings included in the calculation of f above. Therefore, it is a fair statement to make that with the exception of few boron atoms near the outer region of the cluster, all others are part of planar or nearly planar rings, which are however not limited to six-membered but are also eight-membered and larger. This is not in full agreement with the experimental model where the majority of boron atoms are found to be exclusively in six-membered boroxol rings. It remains to be proven with considerably larger models (when these become feasible) whether the larger rings are an artifact of the limited size of the model and will be rearranged into six-membered rings in a much larger model or if the experimental results should be reinterpreted for the presence of larger rings.

2. Vibrational Spectra. ***a. Infrared.*** The vibrational spectra of vitreous B_2O_3 were recorded and analyzed by Galeener et al. in 1980.[18] Two main peaks were identified at 720 and 1260 cm^{-1} in the IR spectrum. A more recent publication[19] reports on the vibrational spectra of a series of doped and undoped borate glasses and summarizes the occurrence of peaks in three regions, the 1200−1450 cm^{-1} region, where B−O stretches of the BO_3 units appear, the 850−1200 cm^{-1} region, where B−O stretches of tetrahedral BO_4 units appear, and the 600−800 cm^{-1} region, where the bending vibrations of the network appear. In the above-mentioned study and in ref 20, it is found that for the undoped B_2O_3 glass, no peaks appear in the middle region, that is, where the tetrahedral B−O stretches should be; the peaks in that region appear and intensify as more doping lithium oxide is added. It is thus concluded that tetrahedral boron atoms exist only when a doping cation is added.

Initial examination of the predicted IR spectra for the three structures that are given in Figure 3 shows a very good agreement with the experimental findings described above. In particular, we note broad peaks in the 600−800 cm^{-1} region for all three structures and also very intense peaks from 1200 to 1600 cm^{-1}, in exactly the same way as the experimental spectra of Galeener[18] and Kamitsos.[20]

It is an appropriate point to note that any theoretical attempt to model the infrared spectrum of a glass will have to make several assumptions and approximations due to the fact that the experimental measurement is of an infrared reflectivity of a solid, whereas the theoretical prediction uses a model of limited size in the gas phase. A further approximation lies in the fact that theory makes a harmonic approximation for what is an anhramonic vibration. However, experience has shown that even under the above-mentioned approximations, many useful results

TABLE 2: Peaks of the Theoretically Predicted RDFs for the Three Structures and Comparison with Experimental Data

	structure I	structure II	structure III	description	experiment[16]	experimental description
ν_1	1.35	1.35	1.35	B−O	1.40	B−O
ν_2	2.35	2.35	2.35	B−B and O−O	2.35	B−B and O−O
ν_3	2.75	2.75	2.65−2.75	B−O	2.70	B−O
ν_4	3.28	3.15	3.28	B−O		
ν_5	3.65	3.65	3.65	B−O	3.60	B−O
ν_6	4.05	4.05	4.05	B−B and O−O	4.05	O−O
ν_7	4.25	4.25	4.25	B−B and O−O		
ν_8	4.65	4.65	4.65	B−O		

are obtained from theory. With this in mind, we can use theoretical data to interpret, and even in some cases exactly reproduce, experimental data.

In this work, we calculate the full force constant matrix within the harmonic approximation for the three models described above using the DFT level of theory with a 6-31G* basis and the HCTH functional. The models, of course, are not symmetric, and therefore, a full set of $3N - 6$ for $N = 100$ vibrational frequencies is calculated; these will not be given here in full (they are available in the Supporting Information, and full force constants are available from the authors), but the 50 frequencies for each structure with the greatest calculated intensities in the infrared are given in Table 3. To graphically represent the calculated infrared spectrum, we use an arbitrary half-width of 50 cm^{-1} (it is noted that theory predicts the integrated infrared intensity for each peak; for presentation reasons, we use Gaussian functions for each peak, with a uniform half-width).

In the theoretical model of structure I, we find a peak at 731 cm^{-1} with a predicted integrated intensity of 337 km/mol and a number of other peaks in that area with intensities over 100 km/mol. These correspond to the experimental peak at 720 cm^{-1}. A similar picture is found in both structures II and III. The peak at 731 cm^{-1} corresponds to a bending vibration of the B−O network, and the same is true for the other peaks up to about 1000 cm^{-1}.

Further, in structure I, we predict a peak at 1277 cm^{-1} with a calculated intensity of 3266 km/mol and a number of other peaks in the region, some with intensities over 1000 km/mol. The 1277 peak corresponds to B−O stretches in rings and is very close to the experimental peak at 1260 cm^{-1}. The same holds for the 1389, 1416, and 1421 cm^{-1} peaks. These peaks, and other less intense ones, all add up to a broad intense band at 1200−1500 cm^{-1}, which is found by the calculated model to be assigned to ring B−O stretching modes. Again, the picture for structures II and III is similar; the individual peaks change

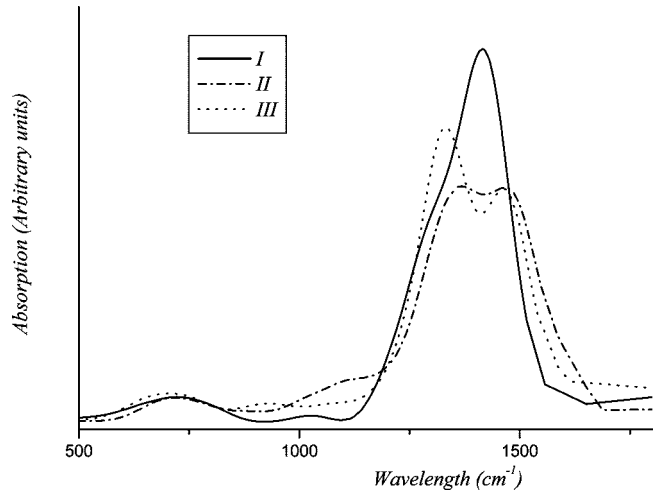

Figure 3. Infrared spectrum composed from theoretical data for the three structures.

TABLE 3: Calculated Frequencies (in cm^{-1}) and Intensities (in km/mol) for the Three Structures[a]

structure I		structure II		structure III	
frequency	intensity	frequency	intensity	frequency	intensity
560	162	901	271	655	191
656	183	1009	388	708	247
731	337	1045	318	753	244
807	180	1082	240	777	203
1027	180	1108	539	907	220
1191	432	1116	271	921	213
1214	1222	1132	464	942	213
1215	327	1180	343	991	306
1238	248	1186	524	1045	207
1250	224	1217	446	1067	286
1263	158	1220	242	1128	322
1269	596	1229	353	1173	336
1277	3266	1258	473	1218	380
1281	262	1275	521	1234	893
1299	480	1277	279	1240	196
1307	1149	1285	575	1248	262
1310	477	1290	572	1265	498
1315	267	1292	529	1268	454
1324	355	1294	317	1277	620
1330	842	1299	254	1282	358
1332	1028	1306	335	1284	307
1340	400	1309	361	1299	721
1347	251	1323	1789	1305	892
1349	435	1335	226	1315	384
1352	761	1339	457	1320	2773
1356	395	1340	1358	1324	1019
1362	398	1359	1993	1330	931
1370	831	1365	806	1334	2767
1377	274	1369	1458	1337	404
1378	402	1375	286	1347	2140
1382	1131	1397	2549	1354	622
1389	2457	1408	282	1361	386
1395	279	1411	1224	1370	810
1398	411	1424	496	1379	1105
1408	887	1446	947	1401	727
1416	2425	1446	393	1409	777
1421	4093	1448	1275	1414	847
1431	1445	1455	345	1420	406
1442	1583	1469	2337	1444	457
1450	1368	1479	720	1451	1468
1452	405	1480	352	1460	656
1460	2585	1487	812	1465	2247
1470	251	1502	2249	1471	2300
1480	837	1510	899	1496	1117
1496	638	1523	2714	1497	1329
1504	294	1548	268	1510	1222
1511	239	1584	852	1521	963
1516	199	1594	1065	1588	636
1557	972	1601	871	1591	539
1651	1187	1653	903	1615	1198

[a] Only the 50 most intense in the infrared are tabulated for each one of the structures.

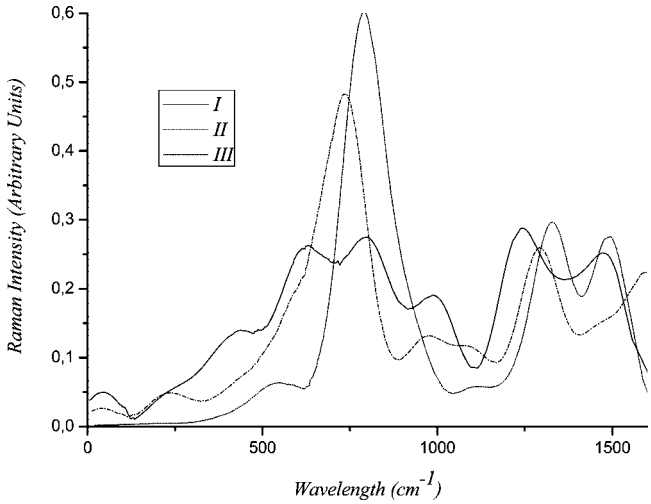

Figure 4. Raman spectrum composed from theoretical data for the three structures.

in position and intensity due to the different environment of the B−O rings, but the overall band remains in the same position and with the same general structure.

Finally, a number of peaks above 1800 cm^{-1} with large intensities are predicted but not included in Figure 3. The reason for this is that these are found to be vibrations involving groups that are at the boundary of the model and hence would not be present in the glass.

b. Raman. The Raman spectrum of vitreous and molten B_2O_3 was reported by Galeener[18] and Walrafen[21] in 1980. The most prominent characteristic is the narrow peak at 801−808 cm^{-1} that is attributed to a "breathing" of the boroxol ring.

The calculated Raman spectrum for the three structures, graphically displayed as described above and with an arbitrary half-width of 60 cm^{-1}, is presented in Figure 4. A vertical shift was necessary for structure III because the absolute values of the Raman activities calculated were considerably higher than those in the other two structures (see Supporting Information). In any case, Raman activities at the DFT level of theory and with a basis set that is designed mainly for structures are not expected to be accurate and are only used as a guide.

The theoretical model of structure I is predicted by the DFT calculation to exhibit a number of closely positioned and very intense Raman lines in the correct region. In particular, the three most intense peaks are found at 798, 803, and 828 cm^{-1}, all with a Raman intensity (always within the harmonic approximation) of 6 $Å^4$/amu; these correspond, as found from the vibrational analysis, to the vibrational analysis to boroxol ring breathing motions, in excellent agreement with the experimental findings. They are closely spaced, and the reason for the small shifts is the different environment in each case; it is reasonable to expect that also in the solid, such small differences of environment will exist but will result in an intense band with a small half-width. We also calculate intense Raman peaks at lower frequencies that are attributed to the "breathing" of larger rings; one such is at 691 cm^{-1} with an intensity of 5 $Å^4$/amu for structure I, but similar ones for the other structures exist. These are also seen in the experimental spectrum and have not to this date been assigned.

Conclusions

We have proven that in a theoretical molecular electronic structure theory model of very good quality, a large enough cluster of vitreous B_2O_3 with no constraints will organize, following energy minimization, in a short-range order consisting of a significant fraction of boroxol rings. Our models also reproduce with good accuracy the infrared and Raman spectra and the radial distribution functions. This means that the spectra can be characterized to a great extent.

Concluding, this study clearly supports a large proportion of planar or nearly planar rings in the structure, the six-membered boroxol being dominant, but also, eight- or even ten-membered rings are found. Further, it is shown that for amorphous materials in general, a large enough model treated to a good level of theory will predict spectra and properties within an excellent degree of accuracy necessary for the interpretation of the experimental results and the determination of the structure. This happens, irrespectively of whether the minima found correspond to the real global minimum of the potential energy surface.

Acknowledgment. Part of this work was carried out under the HPC-EUROPA Project (RII3-CT-2003−506079), with the support of the European Community−Research Infrastructure Action under the FP6 "Structuring the European Research Area" Programme. D.G.L. wishes to acknowledge this grant. Support of this work, in the form of computational resources, was provided through the "Excellence in the Research Institutes" program, supervised by the General Secretariat for Research and Technology, Ministry of Development, Greece (Phase I and II, Projects 64769 and 2005∑E01330081), and is gratefully acknowledged.

Supporting Information Available: Cartesian coordinates and vibrational data. This material is available free of charge via the Internet at http://pubs.acs.org.

References and Notes

(1) Takada, A.; Catlow, C. R. A.; Price, G. D. *J. Phys.: Condens. Matter* **1995**, *7*, 8693.
(2) Micoulaut, M.; Kerner, R.; dos Santos-Loff, D. M. *J. Phys.: Condens. Matter* **1995**, *7*, 8035.
(3) Swenson, J.; Borjesson, L. *Phys. Rev. B* **1997**, *55*, 11138.
(4) Umari, P.; Pasquarello, A. *Phys. Rev. Lett.* **2005**, *95*, 137401.
(5) Swenson, J.; Borjesson, L. *Phys. Rev. Lett.* **2006**, *96*, 199701.
(6) Kashchieva, E.; Shivachev, B.; Dimitriev, Y. *J. Non-Cryst. Solids* **2005**, *351*, 1158.
(7) Zhuang, H.-Z.; Zou, X.-W.; Jin, Z.-Z.; Tian, D.-C. *Phys. Rev. B* **1995**, *52*, 829.
(8) Uchino, T.; Yoko, T. *J. Chem. Phys.* **1996**, *105*, 4140.
(9) Shivachev, B.; Kashchieva, E.; Dimitriev, Y. *Phys. Chem. Glasses* **2005**, *46*, 253.
(10) Simandiras, E. D.; Liakos, D. G. *J. Phys. Chem. A* **2004**, *108*, 3854.
(11) (a) Hamprecht, F. A.; Cohen, A. J.; Tozer, D. J.; Handy, N. C. *J. Chem. Phys.* **1998**, *109*, 6264. (b) Boese, A. D.; Handy, N. C. *J. Chem. Phys.* **2001**, *114*, 5497.
(12) Frisch, M. J. Trucks, G. W.; Schlegel, H. B.; Scuseria, G. E.; Robb, M. A.; Cheeseman, J. R.; Montgomery, J. A., Jr.; Vreven, T.; Kudin, K. N.; Burant, J. C.; Millam, J. M.; Iyengar, S. S.; Tomasi, J.; Barone, V.; Mennucci, B.; Cossi, M.; Scalmani, G.; Rega, N.; Petersson, G. A.; Nakatsuji, H.; Hada, M.; Ehara, M.; Toyota, K.; Fukuda, R.; Hasegawa, J.; Ishida, M.; Nakajima, T.; Honda, Y.; Kitao, O.; Nakai, H.; Klene, M.; Li, X.; Knox, J. E.; Hratchian, H. P.; Cross, J. B.; Bakken, V.; Adamo, C.; Jaramillo, J.; Gomperts, R.; Stratmann, R. E.; Yazyev, O.; Austin, A. J.; Cammi, R.; Pomelli, C.; Ochterski, J. W.; Ayala, P. Y.; Morokuma, K.; Voth, G. A.; Salvador, P.; Dannenberg, J. J.; Zakrzewski, V. G.; Dapprich, S.; Daniels, A. D.; Strain, M. C.; Farkas, O.; Malick, D. K.; Rabuck, A. D.; Raghavachari, K.; Foresman, J. B.; Ortiz, J. V.; Cui, Q.; Baboul, A. G.; Clifford, S.; Cioslowski, J.; Stefanov, B. B.; Liu, G.; Liashenko, A.; Piskorz, P.; Komaromi, I.; Martin, R. L.; Fox, D. J.; Keith, T.; Al-Laham, M. A.; Peng, C. Y.; Nanayakkara, A.; Challacombe, M.; Gill, P. M. W.; Johnson, B.; Chen, W.; Wong, M. W.; Gonzalez, C.; Pople, J. A. *Gaussian 03*, revision C.02; Gaussian, Inc.: Wallingford, CT, 2004.
(13) Phillips, J. C. *J. Non-Cryst. Solids* **1979**, *34*, 153.
(14) Thorpe, M. F. *J. Non-Cryst. Solids* **1983**, *57*, 355.

(15) Boolchand, P.; Thorpe, M. F. *Phys. Rev. B* **1994**, *50*, 10366.
(16) Bursukova, M. A.; Kashchieva, E. P.; Dimitriev, Y. B. *J. Non-Cryst. Solids* **1995**, *192*−*193*, 40.
(17) Liakos, D. G.; Simandiras, E. D. *J. Non-Cryst. Solids* **2008**, *354*, 1569.
(18) Galeener, F. L.; Lukovsky, G.; Mikkelsen, J. C. *Phys. Rev. B* **1980**, *22*, 3983.
(19) Kamitsos, E. I.; Chryssikos, G. D. *J. Mol. Struct.* **1991**, *247*, 1.
(20) Kamitsos, E. I.; Patsis, A. P.; Karakassides, M. A.; Chryssikos, G. D. *J. Non-Cryst. Solids* **1990**, *126*, 52.
(21) Walrafen, G. E.; Samanta, S. R.; Krishnan, P. N. *J. Chem. Phys.* **1980**, *72*, 113.

JP711332K